This is the accepted manuscript made available via CHORUS. The article has been published as:

Linear-in-temperature conductance in two-dimensional electron fluids

Serhii Kryhin, Qiantan Hong, and Leonid Levitov

Phys. Rev. B **111**, L081403 — Published 7 February 2025

DOI: 10.1103/PhysRevB.111.L081403

Linear-in-temperature conductance in two-dimensional electron fluids

Serhii Kryhin, Qiantan Hong and Leonid Levitov
Department of Physics, Massachusetts Institute of Technology, Cambridge, MA 02139

Linear temperature dependence of transport coefficients in metals is often ascribed to non-Fermi-liquid physics. Here we demonstrate the T-linear behavior of nonlocal conductivity in a clean 2D electron fluid, where carrier collisions assist conduction and lead to hydrodynamic transport with conductance rather than resistance growing with temperature. The key aspect is the occurrence of multiple hydrodynamic modes representing odd-parity modulations of the Fermi surface evolving in space and time. A cascade of such modes results in a linear T dependence that extends to lowest temperatures, as well as a Kolmogorov-like fractional power $-5/3$ scaling of conductivity vs. wavenumber. These dependences provide a smoking gun for nonclassical hydrodynamics driven by such modes, expected to be generic for 2D electron fluids with simple near-circular Fermi surfaces.

Unusual temperature dependence of transport properties in metals often hints at exotic physics resulting from electron interactions. A celebrated example is the linear temperature (T) dependence of resistivity observed in many strongly correlated systems, particularly in the vicinity of quantum-critical points[1–8]. Linear T dependence of resistivity that extends to lowest temperatures has become a powerful tool for discerning non-Fermi-liquid phenomena that arise from strong interactions, such as scattering by emergent gauge fields and quantum-critical soft modes of different kinds[9–11]. This stands in contrast with quadratic (T^2) scaling of transport coefficients predicted by conventional Fermi-liquid physics (see [12, 13] and references therein).

Here our aim is to extend these ideas to the domain of electron hydrodynamics[14–42]. Recently it was emphasized that currents in electron fluids are governed by a nonlocal conductivity, featuring a power-law dependence on the wavenumber. Different exponent values have been identified for various regimes [37–40], with the singularity at small wavenumbers indicating the significant role of long-wavelength modes. It is instructive to draw parallels to theories of non-Fermi-liquids, which predict fractional power-law scaling in frequency-dependent optical conductivity, such as $\sigma(\omega) \sim \omega^{-2/3}$ for $\omega \ll E_F$, and establish a connection between this fractional scaling and linear-in-T resistivity [9–11].

In a similar vein, this paper will demonstrate a linear temperature scaling of nonlocal conductivity for two-dimensional electron fluids with simple Fermi surfaces:

$$\sigma(k) \sim Tnk^{-5/3}, \tag{1}$$

where n is carrier density. The Kolmogorov-like fractional power-law dependence in Eq.(1) originates from a cascade of many long-lived modes. For a specific geometry of a constriction (Fig.1) the quantity $\sigma(k)$ defines the conductance upon identifying the constriction width with k^{-1}. This surprising behavior originates from nonclassical hydrodynamics[38] driven by long-lived odd-parity excitations with super-Fermi-liquid decay rates $\gamma_{\rm odd} \sim T^4$ which occur alongside the excitations with normal Fermi-liquid decay rates $\gamma_{\rm even} \sim T^2$ [40, 41]. These excitations create viscous modes with long lifetimes, giving rise to multi-mode electron hydrodynamics.

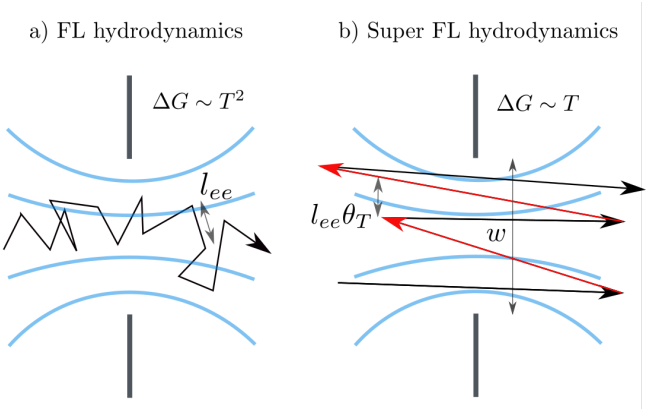


FIG. 1. a), b) Ordinary Fermi-liquid (FL) and unconventional super-Fermi-liquid hydrodynamic flows through a constriction. The FL phase occurs when the ee collision mean free path $l_{\rm ee}$ is smaller than the aperture. In super-FL phase the flow has a very different structure, manifested in a fractional-power divergence in k, Eq.(1). At small T, typical trajectory features many backreflections at small angles $\theta_T \sim T/T_{\rm F}$, allowing particles to propagate out and then return as holes [38, 41]. Conductance behaves as T^2 for FL hydrodynamics and as T for super-FL hydrodynamics, as detailed in Fig.3.

Scaling linear in T is clearly at odds with any analysis perturbative in microscopic rates behaving as T^2 and T^4. As we will see, Eq.(1) is a manifestly non-perturbative result, originating from a cascade encompassing a large family of coupled long-lived modes. It is derived below for circular Fermi surfaces, ignoring momentum relaxation by disorder or phonons, however it holds for all non-circular Fermi surfaces that are convex and possess the $\boldsymbol{p}/-\boldsymbol{p}$ inversion symmetry, which insures the separation of time scales for the even and odd modes. Interestingly, the predicted nonclassical hydrodynamic response holds in a wide range of k extending to values beyond the nominal viscous/ballistic crossover $k\ell_{\rm ee} \sim 1$ (see Fig.3).

Transport measurements in graphene and GaAs constrictions report on resistance decreasing with T [49] and conductance growing with T[50]. In both measurements, the low-T behavior of conductance, which exceeds ballis-

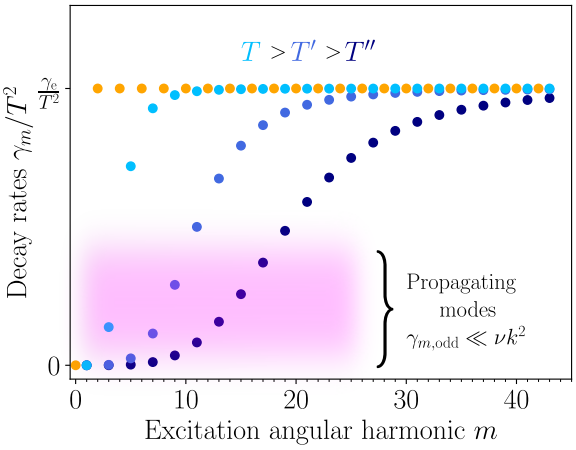


FIG. 2. Decay rates for even and odd excitations, γ_m, vs. harmonic order m, shown as orange and blue dots, respectively [38, 41]. Pictured are rates for three different temperatures $T = 0.1T_{\rm F}$, $T' = 0.01T_{\rm F}$, $T'' = 0.003T_{\rm F}$, with the lighter colors corresponding to higher temperatures. Odd-m rates scale as T^4m^4 for small T and not-too-large m. For large m all rates scale as T^2 independent of the m parity. For interpolation, we used the dependence $\gamma_{m\,\mathrm{odd}} = T^4m^4/(T_{\rm F}^2+m^4T^2)T_{\rm F}^2$. Highlighted in pink are modes with $\gamma_{m\,\mathrm{odd}} \lesssim \nu k^2$, which propagate as weakly damped viscous modes. The number of these modes grows rapidly as T decreases, resulting in a cascade of soft modes and anomalous T dependence of conductance.

tic values seen at $T = 0$, is approximately linear in T. Superballistic conduction is a hallmark of hydrodynamic flow in which ee collisions facilitate conduction. Notably, a linear T dependence that extends to lowest temperatures contradicts the conventional Fermi-liquid picture. This behavior provides a testable signature of the nonclassical hydrodynamics predicted here.

The T-linear scaling contrasts the T^2 scaling expected for the conventional Fermi-liquid hydrodynamics governed by a single viscous mode[14]. In this case, the nonlocal conductivity, obtained from Stokes equation, is

$$\sigma(k) \sim \frac{n}{\nu k^2}, \tag{2}$$

where $\nu = v_F^2/4\gamma_2$ is electrons' kinematic viscosity. For a Fermi liquid, ν scales as $1/T^2$, predicting a T^2 temperature dependence for $\sigma(k)$ and for transport through a constriction shown in Fig.1 [34].

In a realistic geometry such as that shown in Fig.1, the conductance dependence on the aperture width w and temperature can be inferred from the nonlocal conductivity $\sigma(k)$ by setting $k \approx 2\pi/w$. This allows to map out different regimes predicted for $\sigma(k)$ by tuning the lengthscale w. We illustrate the general relation between the k dependence of $\sigma(k)$ and system lengthscale $w \approx 2\pi/k$ by the problem of transport through a long strip, for which a closed-form solution is available [45][46].

The quantities that are central to our analysis of transport mediated by long-lived modes are the eigenvalues γ_m of the linearized collision operator of 2D electrons. The values γ_m give relaxation rates for different angular harmonics of the perturbed Fermi surface,[38, 40, 41, 44]

$$\delta f(\theta) \sim a_m \cos m\theta + b_m \sin m\theta, \tag{3}$$

where θ is the angle on the Fermi surface. Odd-m rates γ_m are much smaller than even-m rates and scale as m^4[38, 44], forming a wide hierarchy of time scales

$$\gamma_{m\,\mathrm{even}} = \gamma, \quad \gamma_{m\,\mathrm{odd}} = \gamma' m^4, \quad m \ll m_*, \tag{4}$$

with the exception of $\gamma_0 = \gamma_1 = 0$ for the density and velocity harmonics $m = 0$ and 1, which are conserved. At $T \ll \epsilon_F$, the rates depend on T as

$$\gamma \sim T^2/\epsilon_F, \quad \gamma' \sim T^4/\epsilon_F^3 \tag{5}$$

such that $\gamma' \ll \gamma$ [40, 41]. Odd-m rates γ_m initially grow as m^4, saturating at the value γ at a large

$$m \gtrsim m_* = (\gamma/\gamma')^{1/4} \tag{6}$$

This hierarchy of even-m and odd-m rates, pictured in Fig.2, demonstrates that the family of long-lived modes, highlighted by pink in Fig.2, quickly grows as temperature decreases. Because of their exceptionally low decay rates, these modes strongly contribute to hydrodynamics.

Our analysis will focus on the nonlocal current-field response due to carrier movement governed by these modes. The response function of interest is nonlocal conductivity

$$j_\alpha(\boldsymbol{x}) = \int d^2x' \sigma_{\alpha\beta}(\boldsymbol{x}-\boldsymbol{x}')E_\beta(\boldsymbol{x}'). \tag{7}$$

Expressed through the k-dependent conductivity as

$$\sigma_{\alpha\beta}(k) = \int d^2x e^{-i\boldsymbol{k}(\boldsymbol{x}-\boldsymbol{x}')}\sigma_{\alpha\beta}(\boldsymbol{x}-\boldsymbol{x}') = \sigma(k)(\delta_{\alpha\beta} - \hat{\boldsymbol{k}}_\alpha\hat{\boldsymbol{k}}_\beta)$$

it plays the same role in the theory of hydrodynamic response as Pippard's nonlocal j vs. A relation in the theory of superconductivity [47] or the nonlocal current-field relation in the theory of the anomalous skin effect [48]. However, unlike these effects, which describe the distribution of supercurrents and normal currents in a narrow surface layer, here the relation in Eq.(7) will be employed to describe current profile in the system bulk.

Fermion kinetics that accounts for perturbed Fermi surface dynamics yields a general closed-form solution for hydrodynamic conduction. This is achieved by linking the transverse conductivity $\sigma_{\alpha\beta}(k) = \sigma(k)(\delta_{\alpha\beta} - \hat{\boldsymbol{k}}_\alpha\hat{\boldsymbol{k}}_\beta)$ to a quantity $\Gamma(k)$ defined as a continued fraction comprised of γ_m rates [36, 45]

$$\sigma(k) = \frac{D}{\gamma_p + \frac{z}{\Gamma(k)}}, \quad \Gamma(k) = \gamma_2 + \frac{z}{\gamma_3 + \frac{z}{\gamma_4 + \frac{z}{\gamma_5 + \cdots}}}. \tag{8}$$

Here $z = v_F^2k^2/4$ and $D = ne^2/m$ is the Drude weight, where we expressed carrier density through Fermi momentum, $n = gp_F^2/4\pi\hbar^2$, with g the spin/valley degeneracy. The quantity $\Gamma(k)$ can be referred to as 'hydrodynamic conductance'. Indeed, in the ideal fluid phase, i.e.

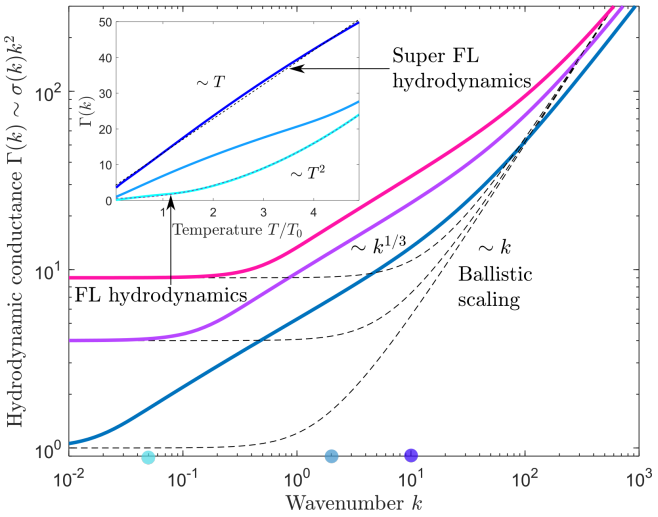


FIG. 3. Scale-dependent conductance $\Gamma(k) \sim \sigma(k)k^2$, Eq.(8), shown as a function of k and T for the rates γ_m given in Fig. 2. Main panel: $\Gamma(k)$ at three distinct temperatures T_0, $2T_0$, $4T_0$ (blue, purple and red curves) shown for $T_0 \approx 2.5 \cdot 10^{-3} T_{\rm F}$. The wavenumber k is given in the units of $k_0 = \gamma(T_0)/v_F$, obtained for $\gamma(T)$ taken at temperature T_0. The k dependence features distinct regimes: Fermi-liquid (FL) and super FL hydrodynamic phases, in which $\Gamma(k)$ is k-independent and scales as $k^{1/3}$, respectively. As a comparison, $\Gamma(k)$ for conventional Gurzhi FL hydrodynamics is shown by dashed lines for matching parameter values (see discussion in text). Inset: T dependence in these phases obtained for three k values marked on the x axis (these are taken in the FL, super FL and an intermediate phase—cyan, blue and light blue curves and dots). Temperature scaling, T for super FL and T^2 for FL regimes, is validated by best fits to a linear and quadratic T dependence (dashed lines, inset).

in the absence of momentum relaxing scattering, $\gamma_p = 0$, the conductivity $\sigma(k)$ equals $(D/z)\Gamma(k)$.

The properties of $\Gamma(k)$ are sensitive to the even/odd parity asymmetry and m dependence in γ_m. In Fig.2 we present numerical results for $\Gamma(k)$ obtained from the rates given in Eq.(4) The dependence $\Gamma(k)$ vs. k exhibits three distinct regimes. Fermi-liquid hydrodynamics occurs at the smallest k. Here $\Gamma(k)$ is k-independent, giving conductivity scaling $\sigma(k) \sim 1/k^2$, as expected for linearized Navier-Stokes equation. In the 'super-FL hydrodynamics' phase $\Gamma(k)$ obeys power-law scaling $k^{1/3}$. Temperature dependence of $\Gamma(k)$, shown in the inset, is T^2 in the first regime, as expected for FL. Yet, a linear T dependence emerges in the super-FL phase, a surprising behavior explained below (see Eqs.(1),(2)). At even higher k a ballistic regime sets in, with $\Gamma(k)$ linear in k and temperature-independent. Notably, the T-dependent part of $\Gamma(k)$, while being small at large k, remains linear, explaining the robustness of the T-linear scaling even at lowest temperatures.

As evident in Fig.3, the range of k in which super-FL regime occurs grows as temperature decreases. This behavior can be understood as follows. At small k the super-FL regime is bordered by a crossover to Gurzhi's FL hydrodynamics. The crossover occurs at $k \approx \kappa_<$ corresponding to distances over which the longest-lived odd-m excitation, namely the $m = 3$ harmonic, travels over its lifetime. This gives a condition $\gamma_3 = \nu\kappa_<^2$. On the large k side it is bordered by a crossover from super FL to the ballistic regime. A simple estimate for this crossover is provided by a toy model [45] in which γ_m for m_* lowest odd-m modes are neglected, whereas for $m > m_*$ the odd-m and even-m rates are taken to be equal. In this model the conductivity at small k behaves as $\sigma_{\rm sFL}(k) = \frac{m_*+1}{\nu k^2} D$. We set m_* to the value at which the even/odd asymmetry disappears, Eq.(6). The crossover position $k_>$ is then determined by the condition $\sigma_{\rm sFL}(k) = \frac{D}{v_F k}$. This gives the domain of existence of the super FL regime

$$\kappa_< < k < \kappa_>, \quad \kappa_< = \frac{(\gamma\gamma')^{1/2}}{v_F}, \quad \kappa_> = \frac{\gamma^{5/4}}{v_F \gamma'^{1/4}}. \tag{9}$$

Since at low temperatures the rates γ and γ' scale as T^2 and T^4, the quantities $\kappa_<$ and $\kappa_>$ scale as T^3 and $T^{3/2}$, respectively. This explains widening of the super FL regime at low T. These estimates, as will be seen below, agree with the exact analytic result for $\sigma(k)$ scaling.

As a comparison, $\Gamma(k)$ for FL hydrodynamics is shown in Fig.3 (main panel, dashed lines). The T dependence is absent in the ballistic regime and is T^2 in the FL regime. Notably, the k-linear behavior at large k, describing ballistic transport, is pushed to high k in the super FL regime. This indicates that the super FL regime is readily accessible for realistic system widths.

Next, we present an analytic approach that allows to evaluate $\Gamma(k)$ and derive the T-linear and $k^{-5/3}$ scaling for super FL given in Eq.(1). We first briefly consider an artificial case when all γ_m take identical values $\gamma_m = \gamma$ $(m > 1)$ with no even/odd asymmetry. In this case evaluating the continued fraction yields $\sigma(k)$ of the form in Eq.(8) with $\Gamma(k) = (\gamma + \sqrt{\gamma^2 + 4z^2})/2$. In the long-wavelength limit $kv_F \ll \gamma$, the term $4z^2$ under the square root can be ignored, giving a result identical to that found from Stokes hydrodynamics, $\sigma(k) = D/(\gamma_p + z/\gamma)$. This quantity features a T^2 scaling at $\gamma_p = 0$, Eq.(2).

A very different behavior arises for the rates with an even/odd asymmetry. This problem is considerably more challenging, in particular because odd-m rates depend on m, with large differences between successive even and odd m occurring at $m < m_*$, Eq.(4). First, to capture this behavior in a simplified model, we set $\gamma_m = \gamma_{\rm e}$ for all even m and $\gamma_{\rm o}$ for all odd m, ignoring the m dependence of $\gamma_{\rm e}$ and $\gamma_{\rm o}$. In this case, $\Gamma(k)$ can be evaluated exactly:

$$\Gamma(k) = \frac{1}{2}\sqrt{\frac{\gamma_{\rm e}}{\gamma_{\rm o}}}\left(\sqrt{\gamma_{\rm o}\gamma_{\rm e}} + \sqrt{\gamma_{\rm o}\gamma_{\rm e} + k^2 v_F^2}\right). \tag{10}$$

This motivates introducing "level-m" partial continued fractions, defined as

$$\Gamma_m(k) = \gamma_m + \frac{z}{\gamma_{m+1} + \frac{z}{\gamma_{m+2}+\cdots}}. \tag{11}$$

These quantities, evaluated similarly, are

$$\Gamma_m(k) = b_m(\sqrt{\gamma_o\gamma_e} + \sqrt{\gamma_o\gamma_e + k^2 v_F^2})/2, \qquad (12)$$

with $b_{m\,\mathrm{even}} = \sqrt{\gamma_e/\gamma_o}$ and $b_{m\,\mathrm{odd}} = \sqrt{\gamma_o/\gamma_e}$. When the even/odd difference is significant, $\gamma_e \gg \gamma_o$, the quantities Γ_m are much larger for even m than for odd m.

Below, we upgrade this picture in order to treat the quasi-continuum of weakly decaying modes highlighted in pink in Fig.2. At low T, despite the even/odd beating effect, Γ_m is slowly varying with m for each individual parity of m. It is then natural to analyze the dependence Γ_m vs. m for a fixed parity. The result for $\Gamma(k)$ can then be found by taking $\Gamma_{m=2}$ [46]. This analysis predicts an exact fractional-power-law scaling relation for $\Gamma(k)$:

$$\Gamma(k) = \frac{A\gamma}{(\gamma\gamma')^{\frac{1}{6}}}\left(\frac{kv_F}{2}\right)^{\frac{1}{3}}, \quad A = \frac{\Gamma(\frac{1}{6})}{12^{\frac{2}{3}}\Gamma(\frac{5}{6})} \approx 0.94. \quad (13)$$

From the temperature dependence of the rates $\gamma \sim T^2$ and $\gamma' \sim T^4$, the resulting T dependence of $\Gamma(k)$ is linear,

$$\Gamma(k) \sim Tk^{1/3}. \qquad (14)$$

Eq.(8) then yields $\sigma(k) = D/\left(\gamma_p + A'k^{5/3}/T\right)$ with A' a T-independent factor. The dependence on the wavenumber k translates into a dependence on system geometry. In the presence of momentum relaxing scattering due to phonons, in which case $\gamma_p \sim T$, the expected T dependence becomes nonmonotonic, growing at low T, where ee scattering dominates, and decreasing at elevated T.

To derive the scaling relation given in Eq.(13), we perform the recursion analysis of partial continued fractions, Eq.(11), focusing on the even-m quantities Γ_m. Taking a difference of Γ_m and Γ_{m+2}, and using Eq.(11) yields

$$\Gamma_m - \Gamma_{m+2} = \gamma_m - \frac{\gamma_{m+1}\Gamma_{m+2}^2}{\gamma_{m+1}\Gamma_{m+2} + z} \qquad (15)$$

It turns out, perhaps surprisingly, that this exact nonlinear relation is greatly simplified through the substitution

$$\Gamma_m = \frac{z}{\gamma_{m-1}}\left(\frac{u_m}{u_{m+2}} - 1\right). \qquad (16)$$

After this substitution Eq.(15) yields linear relations

$$\frac{z}{\gamma_{m+1}}u_{m+4} + \frac{z}{\gamma_{m-1}}u_m = \left(\gamma_m + \frac{z}{\gamma_{m-1}} + \frac{z}{\gamma_{m+1}}\right)u_{m+2},$$

which represents a discrete second-order ODE for u_m. At low T, γ_m and u_m are slowly varying functions of m in the region marked in pink in Fig.1. The analysis based on slowly varying variables u_m describes a cascade of modes that propagate, slowly decay and interact with each other. In this case, the discrete ODE can be taken to the continuous domain, giving a Bessel equation that can be readily solved to obtain $\Gamma(k)$ given in Eq.(13) [46].

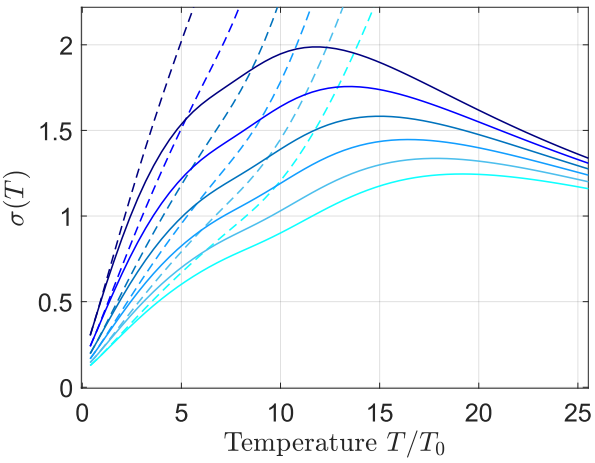


FIG. 4. Nonmonotonic T dependence of conductivity arising in the presence of el-ph scattering [see Eqs.(8),(20)]. At low temperatures $T < T_{\mathrm{BG}}$ the el-ph scattering vanishes rapidly, giving negligible contribution to momentum relaxation, whereas at $T > T_{\mathrm{BG}}$ the momentum relaxation rate grows and dominates conductivity. Accordingly, the conductivity grows linearly with T at low temperatures and decreases at higher temperatures (see text). Shown are curves obtained for wavenumbers $k/k_0 = 10$, 12, 14, 16, 18 and 20, where lighter colors correspond to smaller wavenumbers. The wavenumber and temperature units k_0 and T_0 are the same as in Fig.3. Dashed lines represent the conductivity in the absence of el-ph scattering, $\gamma_p = 0$. For illustration, the Bloch-Grüneisen temperature was taken to be $T_{\mathrm{BG}} = 6T_0$.

Importantly, the transformation to a continuous domain is only valid when $|u'(m)/u(m)| \ll 1$. It is therefore applicable in some of the transport regimes but fails in other regimes. For instance, the conventional hydrodynamic regime, which occurs at small wavenumbers k, is dominated by the $m = 1$ velocity mode, whereas $u_{m>1}$ are negligible. It is therefore not described by u_m which is quasi-continuous in m. Likewise, in the ballistic regime, which occurs at large enough k, the relevant harmonics encompass m far outside the pink region in Fig.1 where $\gamma_{\mathrm{odd}} \ll \gamma_{\mathrm{even}}$. In contrast, the super-FL regime, describing the cascade of many long-lived modes, is captured well by the quasi-continuous approximation.

Lastly, the knowledge of conductivity as a function of k and T can be used to predict transport coefficients for realistic geometry. As an illustration, we consider transport in a strip of width w and length $\ell \gg w$. In this limit, we have an exact relation between the strip conductance $G = 1/R$ and the nonlocal conductivity $\sigma(k)$ [46]:

$$G = \frac{1}{\ell}\sum_{n=\pm1,\pm2\ldots}\sigma(k_n), \quad k_n = 2\pi n/w. \qquad (17)$$

As a sanity check, for $\sigma(k) = D/\nu k^2$ (the conventional viscous regime) Eq.(17) predicts scaling expected for Poiseuille flow, $G \sim DT^2w^3/\nu L$. At $w \approx \ell$ this result agrees with expectations for viscous transport in

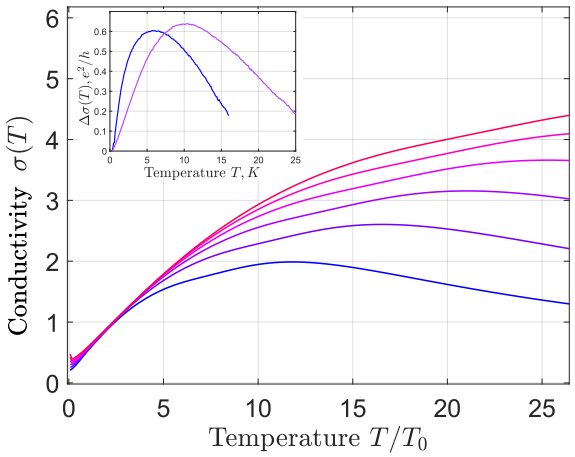


FIG. 5. Nonmonotonic T dependence of conductivity, obtained as in Fig.4, shown for several carrier density values: $n/n_0 = 1.0$, 1.5, 2.0, 2.5, 3.0, and 3.5, where $n_0 = (gm/2\pi\hbar^2)T_{\rm F}$ corresponds to the carrier density at the Fermi energy $T_{\rm F}$. The warmer colors correspond to higher densities. and a fixed $k/k_0 = 10$ was assumed. The density dependence for the physical quantities used in Eq.(8) was taken to be $D \sim n$, $v_F \sim \sqrt{n}$, $k_{\rm F} \sim \sqrt{n}$, $T_{\rm F} \sim n$, and $T_{\rm BG} \sim \sqrt{n}$, which matches the dependence $T_{\rm BG} \approx sk_{\rm F}$. Inset shows conductance temperature dependence reported in Ref.[50], measured in constrictions formed in split-gated GaAs electron systems. The two curves represent the T-dependent part of conductance obtained for two different carrier density values [51].

constrictions [34]. In the super-FL regime described by $\sigma(k) \sim \frac{T}{k^{5/3}}n$, Eq.(1), the strip conductance behaves as

$$G \sim \frac{Tw^{\frac{8}{3}}}{\ell}n. \tag{18}$$

At $L \approx w$ this yields $w^{5/3}$ scaling that agrees with the nonlocal conductivity scaling $k^{-5/3}$ derived above. It also matches the quantity $\sigma(k,T)$ with k linked to the strip width as $k \sim w^{-1}$. Combined with the existence conditions for the super-FL regime in Eq.(9), this defines a range of strip widths at which this regime can occur:

$$\frac{T^3}{T_{\rm F}^2} \lesssim \frac{\hbar v_F}{w} \lesssim T\sqrt{\frac{T}{T_{\rm F}}}. \tag{19}$$

The temperature interval in which the super-FL phase occurs rapidly widens as T decreases.

Next, we demonstrate that the T-linear behavior of $\sigma(k)$ at low temperatures remains robust in the presence of electron-phonon (el-ph) scattering. The reason for such robustness is that the rates of momentum-relaxing el-ph processes quickly diminish at low temperatures. For 2D electron systems, microscopic analysis predicts relaxation rates vanishing as $\gamma_m \sim T^7 m^2$ at temperatures below the Bloch-Grüneisen temperature, $T < T_{\rm BG} \simeq sk_{\rm F}$, where s is sound velocity [57]. At these temperatures, because of the T^7 dependence, the el-ph rates are subleading to the el-el rates which govern the super-FL hydrodynamics. However, the el-ph rates become significant at $T \gtrsim T_{\rm BG}$, scaling linearly with T as temperature grows. As a result, at elevated T the el-ph rates dominate the el-el rates, resulting in conductivity decreasing with temperature. This nonmonotonic T dependence of conductivity, which is illustrated in Figs. 5 and 4, can be described by our continued fraction model, Eq.(8), by incorporating the el-ph rates γ_p in the rates γ_m as

$$\gamma_m \to \gamma_m + \gamma_p. \tag{20}$$

Following Refs.[57], we model the temperature dependence of γ_p by an expression

$$\gamma_p \sim \left(\frac{T}{T_{\rm BG}}\right)^7 \int_0^{T_{\rm BG}/T} dt \frac{t^7}{(e^t-1)(1-e^{-t})}, \tag{21}$$

valid at T both larger and smaller than $T_{\rm BG}$ (but excluding the m^2 dependence in the low temperature regime for simplicity). At such temperatures, γ_p behaves at T and $T^7/T_{\rm BG}^6$, respectively. Incorporating γ_p into γ_m impacts conductivity as illustrated in Figs.5 and 4: the linear-in-T conductivity growth at low T remains robust, with the linear behavior extending to lowest T. In contrast, at higher T, the sign of conductivity T dependence is reversed, giving a nonmonotonic behavior which agrees with experimental observations reported in Refs.[49, 50]

In summary, conductivity growing with temperature is a hallmark of the hydrodynamic regime in which ee collisions facilitate conduction and suppress dissipation. In contrast to the conventional FL hydrodynamics, which predicts conductivity growing as T^2 at $T \ll T_{\rm F}$, the super-FL conductance grows more rapidly, increasing linearly with temperature. The enhanced conductance reflects presence of multiple long-lived modes unique to 2D fermions. Recently, conductance exceeding the ballistic $T = 0$ value and growing linearly with T has been observed for superballistic transport in graphene and GaAs electron fluids [49, 50]. This indicates that ongoing experiments [52–56] are well positioned to probe the exotic hydrodynamics driven by emergent long-lived modes. Further, we expect similar anomalous T-dependent hydrodynamic effects in strongly-correlated systems that host soft quantum-critical modes or emergent gauge fields [1–11] activated at low temperatures.

We are grateful to Klaus Ensslin, Andre Geim, Lev Ginzburg and Boris Spivak for useful discussions. This work was supported by the Science and Technology Center for Integrated Quantum Materials, National Science Foundation grant No. DMR1231319 and was performed in part at Aspen Center for Physics, which is supported by NSF grant PHY-2210452. SK is currently affiliated with Harvard University, Physics Department.

[1] S. Sachdev, B. Keimer, Quantum Criticality, Physics Today 64, 2, 29 (2011)

[2] P. W. Phillips, N. E. Hussey, P. Abbamonte, Stranger than metals, Science 377, 169 (2022)

[3] C. M. Varma, Colloquium: Linear in temperature resistivity and associated mysteries including high temperature superconductivity. Rev. Mod. Phys. 92, 031001 (2020).

[4] C. M. Varma, P. B. Littlewood, S. Schmitt-Rink, E. Abrahams, A. E. Ruckenstein, Phenomenology of the normal state of Cu-O high-temperature superconductors. Phys. Rev. Lett. 63, 1996 (1989).

[5] C. Proust, L. Taillefer, The remarkable underlying ground states of cuprate superconductors. Annu. Rev. Condens. Matter Phys. 10, 409-429 (2019).

[6] S. A. Hartnoll, A. P. Mackenzie, Colloquium: Planckian dissipation in metals. Rev. Mod. Phys. 94, 041002 (2022).

[7] J. Zaanen, Planckian dissipation, minimal viscosity and the transport in cuprate strange metals. SciPost Phys. 6, 061 (2019).

[8] S. A. Hartnoll, Theory of universal incoherent metallic transport. Nat. Phys. 11, 54-61 (2015).

[9] H. Guo, A. A. Patel, I. Esterlis, and S. Sachdev, Large-N theory of critical Fermi surfaces. II. Conductivity, Phys. Rev. B 106, 115151 (2022).

[10] P. A. Lee, Gauge Field, Aharonov-Bohm Flux, and High-T_c Superconductivity, Phys. Rev. Lett. 63, 680 (1989).

[11] Y. B. Kim, A. Furusaki, X.-G. Wen, and P. A. Lee, Gauge-invariant response functions of fermions coupled to a gauge field, Phys. Rev. B 50, 17917 (1994).

[12] X. Lin, B. Fauque and K. Behnia, Science 349, 945-948 (2015).

[13] H. K. Pal, V. I. Yudson and D. L. Maslov, Resistivity of non-Galilean-invariant Fermi- and non-Fermi liquids, Lith. J. Phys. 52, 142-164 (2012).

[14] R. N. Gurzhi, Sov. Phys. Usp. 11, 255 (1968). DOI 10.1070/PU1968v011n02ABEH003815

[15] M. Müller, J. Schmalian, L. Fritz, Graphene: a nearly perfect fluid. Phys. Rev. Lett. 103, 2–5 (2009).

[16] A. Tomadin, G. Vignale, M. Polini, A Corbino disk viscometer for 2D quantum electron liquids Phys. Rev. Lett. 113, 235901 (2014).

[17] A. Principi, G. Vignale, M. Carrega, M. Polini, Bulk and shear viscosities of the two-dimensional electron liquid in a doped graphene sheet Phys. Rev. B 93, 125410 (2016)

[18] T. Scaffidi, N. Nandi, B. Schmidt, A. P. Mackenzie, J. E. Moore, Hydrodynamic electron flow and Hall viscosity. Phys. Rev. Lett. 118, 226601 (2017).

[19] A. Lucas, K. C. Fong, Hydrodynamics of electrons in graphene, J. Phys.: Condens. Matter 30 053001 (2018).

[20] K. A. Guerrero-Becerra, F. M. D. Pellegrino, M. Polini, Magnetic hallmarks of viscous electron flow in graphene. Phys. Rev. B 99, 041407 (2019).

[21] B. N. Narozhny, M. Schütt, Magnetohydrodynamics in graphene: Shear and Hall viscosities. Phys. Rev. B 100, 035125 (2019).

[22] G. Wagner, D. X. Nguyen and S. H. Simon, Transport in Bilayer Graphene near Charge Neutrality: Which Scattering Mechanisms Are Important? Phys. Rev. Lett. 124, 026601 (2020).

[23] S. Li, A. Levchenko and A. V. Andreev, Hydrodynamic electron transport near charge neutrality, Phys. Rev. B 102, 075305 (2020)

[24] A. Levchenko and J. Schmalian, Transport properties of strongly coupled electron–phonon liquids, Annals of Physics 419, 168218 (2020).

[25] A. G. Abanov, T. Can, S. Ganeshan, G. M. Monteiro, Hydrodynamics of two-dimensional compressible fluid with broken parity: variational principle and free surface dynamics in the absence of dissipation, Phys. Rev. Fluids 5, 104802 (2020)

[26] P. S. Alekseev, A. P. Dmitriev, Viscosity of two-dimensional electrons. Phys. Rev. B 102, 241409 (2020).

[27] R. Toshio, K. Takasan, N. Kawakami, Anomalous hydrodynamic transport in interacting noncentrosymmetric metals. Phys. Rev. Res. 2, 032021 (2020).

[28] B. N. Narozhny, I. V. Gornyi, M. Titov, Hydrodynamic collective modes in graphene. Phys. Rev. B 103, 115402 (2021).

[29] E. H. Hasdeo, J. Ekstrom, E. G. Idrisov, T. L. Schmidt, Electron hydrodynamics of two-dimensional anomalous Hall materials. Phys. Rev. B 103, 125106 (2021).

[30] M. Qi, A. Lucas, Distinguishing viscous, ballistic, and diffusive current flows in anisotropic metals, Phys. Rev. B 104 (19), 195106 (2021)

[31] C. Q. Cook, A. Lucas, Viscometry of electron fluids from symmetry, Phys. Rev. Lett. 127 (17), 176603 (2021)

[32] D. Valentinis, J. Zaanen, D. van der Marel Propagation of shear stress in strongly interacting metallic Fermi liquids enhances transmission of terahertz radiation Sci. Rep. 11, 7105 (2021)

[33] D. Valentinis, Optical signatures of shear collective modes in strongly interacting Fermi liquids Phys. Rev. Research 3, 023076 (2021)

[34] H. Guo, E. Ilseven, G. Falkovich, and L. Levitov, Higher-than-ballistic conduction of viscous electron flows, Proc. Natl. Acad. Sci. U.S.A. 114, 3068 (2017).

[35] A. V. Shytov, J. F. Kong, G. Falkovich, and L. S. Levitov, Particle Collisions and Negative Nonlocal Response of Ballistic Electrons, Phys. Rev. Lett. 121, 176805 (2018).

[36] K. G. Nazaryan, L. S. Levitov, Nonlocal conductivity, continued fractions and current vortices in electron fluids, arXiv:2111.09878.

[37] E. I. Kiselev, J. Schmalian, Lévy flights and hydrodynamic superdiffusion on the Dirac cone of Graphene, Phys. Rev. Lett. 123, 195302 (2019).

[38] P. Ledwith, H. Guo, A. Shytov, L. Levitov Tomographic Dynamics and Scale-Dependent Viscosity in 2D Electron Systems, Phys. Rev. Lett. 123, 116601 (2019).

[39] X. Huang and A. Lucas, Fingerprints of quantum criticality in locally resolved transport, SciPost Phys. 13 004 (2022).

[40] J. Hofmann and S. Das Sarma, Collective modes in interacting two-dimensional tomographic Fermi liquids, Phys. Rev. B 106, 205412 (2022).

[41] S. Kryhin, L. Levitov, Collinear scattering and long-lived excitations in two-dimensional electron fluids, Phys. Rev. B 107, L201404 (2023); arXiv preprint arXiv:2112.05076 (2021).

[42] J. Hofmann, U. Gran, Anomalously long lifetimes in two-dimensional Fermi liquids, arXiv preprint arXiv:2210.16300 (2022)

[43] P. J. Ledwith, H. Guo, L. Levitov, Angular Superdiffusion and Directional Memory in Two-Dimensional Electron Fluids, arXiv:1708.01915

[44] P. J. Ledwith, H. Guo, L. Levitov, The Hierarchy of Excitation Lifetimes in Two-Dimensional Fermi Gases, Ann. Phys. 411, 167913 (2019).

[45] S. Kryhin, L. Levitov, Non-Newtonian hydrodynamic modes in two-dimensional electron fluids, preprint arXiv:2305.02883

[46] Supplemental information uses the approach introduced in Ref.[45] to illustrate the relation between the nonlocal conductivity $\sigma(k)$ and the dependence of transport on system geometry and temperature. It also provides technical details of the solution of the discrete ODE in the super-FL cascade response regime.

[47] M. Tinkham, Introduction to Superconductivity (Dover Books on Physics, 1996).

[48] L. P. Pitaevskii, E. M. Lifshitz, Physical Kinetics, (Butterworth-Heinemann, 1981)

[49] R. Krishna Kumar, D. A. Bandurin, F. M. D. Pellegrino, Y. Cao, A. Principi, H. Guo, G. H. Auton, M. Ben-Shalom, L. A. Ponomarenko, G. Falkovich, K. Watanabe, T. Taniguchi, I. V. Grigorieva, L. S. Levitov, M. Polini, and A. K. Geim, Superballistic flow of viscous electron fluid through graphene constrictions, Nature Physics 13, 1182 (2017).

[50] L. V. Ginzburg, Y. Wu, M. P. Roosli, P. R. Gomez, R. Garreis, C. Tong, V. Stará, C. Gold, K. Nazaryan, S. Kryhin, H. Overweg, C. Reichl, M. Berl, T. Taniguchi, K. Watanabe, W. Wegscheider, T. Ihn, K. Ensslin, Long distance electron-electron scattering detected with point contacts, arXiv:2308.06056

[51] The data shown in Fig.4 inset represents experimental curves $G(T) - G(T = 0)$, measured directly at zero magnetic field, as reported in Ref. [50]. For comparison, the same data is presented in Ref.[50], Fig. 5, after subtracting a $|B|$ dependence.

[52] J. A. Sulpizio, L. Ella, A. Rozen, J. Birkbeck, D. J. Perello, D. Dutta, M. Ben-Shalom, T. Taniguchi, K. Watanabe, T. Holder, R. Queiroz, A. Principi, A. Stern, T. Scaffidi, A. K. Geim, S. Ilani, Visualizing Poiseuille flow of hydrodynamic electrons, Nature 576, 75-79 (2019).

[53] M. J. H. Ku, T. X. Zhou, Q. Li, Y. J. Shin, J. K. Shi, C. Burch, L. E. Anderson, A. T. Pierce, Y. Xie, A. Hamo, U. Vool, H. Zhang, F. Casola, T. Taniguchi, K. Watanabe, M. M. Fogler, P. Kim, A. Yacoby, R. L. Walsworth, Imaging viscous flow of the Dirac fluid in graphene, Nature 583, 537-541 (2020).

[54] B. A. Braem, F. M. D. Pellegrino, A. Principi, M. Roosli, C. Gold, S. Hennel, J. V. Koski, M. Berl, W. Dietsche, W. Wegscheider, M. Polini, T. Ihn, and K. Ensslin, Scanning gate microscopy in a viscous electron fluid, Phys. Rev. B 98, 241304(R) (2018).

[55] U. Vool, A. Hamo, G. Varnavides, Y. Wang, T. X. Zhou, N. Kumar, Y. Dovzhenko, Z. Qiu, C. A. C. Garcia, A. T. Pierce, J. Gooth, P. Anikeeva, C. Felser, P. Narang, A. Yacoby, Imaging phonon-mediated hydrodynamic flow in WTe2, Nature Physics 17, 1216-1220 (2021).

[56] A. Aharon-Steinberg, T. Volkl, A. Kaplan, A. K. Pariari, I. Roy, T. Holder, Y. Wolf, A. Y. Meltzer, Y. Myasoedov, M. E. Huber, B. Yan, G. Falkovich, L. S. Levitov, M. Hucker, E. Zeldov, Direct observation of vortices in an electron fluid, Nature 607, 74-80 (2022).

[57] H. L. Stormer, L. N. Pfeiffer, K. W. Baldwin, and K. W. West, Observation of a Bloch-Grüneisen regime in two-dimensional electron transport, Phys. Rev. B 41, 1278(R) (1990).